Chemical Geology xxx (xxxx) 121456

Contents lists available at ScienceDirect

Chemical Geology

journal homepage: www.elsevier.com/locate/chemgeo

Oceanic redox conditions during the terminal Cambrian extinction event

Xi Chen [a, b, *], Graham A. Shields [b], Morten B. Andersen [c], Chen Qiu [a], Si-Yu Min [a], Qing-Feng Shao [d], Hong-Fei Ling [a]

[a] Laboratory for Mineral Deposits Research, School of Earth Sciences and Engineering, Nanjing University, Nanjing 210023, China
[b] Department of Earth Sciences, University College London, London WC1E 6BT, UK
[c] School of Earth and Environmental Sciences, Cardiff University, Cardiff CF10 3AT, UK
[d] Key Laboratory of Virtual Geographic Environment, Nanjing Normal University, Nanjing 210023, China

ARTICLE INFO

Editor: Michael E. Boettcher

Keywords:
Uranium isotopes
TOCE
Suboxic
OMZ
Intermediate reducing
End-Ptychaspid Biomere extinction

ABSTRACT

Marine animal diversity during the late Cambrian was reduced by a series of extinctions that have generally been attributed to oceanic anoxic events associated with positive carbon isotope excursions. Here we present carbon and uranium isotope ratios ($\delta^{13}C$ and $\delta^{238}U$ values) as proxies for global carbon cycle and oceanic redox conditions, respectively, from carbonate rocks of the Wa'ergang section, South China. The dataset spans an interval that includes the last major negative $\delta^{13}C$ excursion (TOCE) of the Cambrian Period. The TOCE is a globally documented event, recovery from which corresponds to the terminal Cambrian extinction event. The $\delta^{13}C$ and $\delta^{238}U$ values covary through the section, shifting initially to lower values, with $\delta^{238}U$ falling below the modern open-ocean seawater value from the start to the middle of the profile, followed by a shift to higher values towards the end of the Cambrian. Neither the co-occurrence of $\delta^{13}C$ and $\delta^{238}U$ negative excursions, nor the association of rising $\delta^{238}U$ with extinction have been commonly reported. Here we argue that robust positive coupling of $\delta^{13}C$ and $\delta^{238}U$ relates to the existence of extensive intermediate reducing settings (from low-O_2 suboxia to intermittent anoxia) during the late Cambrian alongside low atmospheric pO_2 and a greenhouse climate. Similarly, a stepwise increase in the $\delta^{238}U$ baseline in carbonates across the Ediacaran–Cambrian boundary is consistent with the growing importance of an intermediate reducing sink through that interval. We propose further that divergent trends in lower and upper ocean redox conditions could have driven the parallel isotope excursions. An expansion of intermediate reducing conditions, rather than persistent anoxic euxinia, is consistent with the recovery of $\delta^{13}C$ and $\delta^{238}U$ to higher values, as well as the presence of benthic fauna and shoreward extension of deeper-water fauna that may have had a greater tolerance against hypoxia.

1. Introduction

The major body plans (phyla) of animals were already established during the early Cambrian bioradiations ('Cambrian Explosion'), although available marine ecospace would not be filled to capacity until the Late Ordovician (Sheehan, 2001) and animal diversity suffered repeated extinctions after the 'Cambrian Explosion' (Palmer, 1984; Zhuravlev, 2001). During the Furongian Epoch (497–485.4 Ma, the last Cambrian epoch), marine invertebrate fossil diversity decreased particularly significantly during the so-called 'Furongian Gap' (Harper et al., 2019). This interval comprises three major extinction events separating suprazonal biostratigraphic units named 'biomeres' (Palmer, 1965; Stitt, 1971; Palmer, 1984; Taylor, 2006). Sea-level changes, cooling, upwelling, and anoxic events have all been proposed as possible triggers for those extinctions (Palmer, 1984; Taylor, 2006; Gill et al., 2011; Saltzman et al., 2015).

The youngest Cambrian extinction event, the end-Ptychaspid Biomere extinction, occurred within the last Cambrian stage. Like other end-of-biomere extinctions, it was first recognized on the Laurentian shelf where trilobites experienced major and rapid turnover (Stitt, 1971; Palmer, 1984). This extinction was subsequently shown to also affect conodonts and brachiopods simultaneously (Miller et al., 2006; Freeman et al., 2018). Although there has been a lack of paleontological studies on the global occurrences of this specific end-of-biomere extinction, the earlier end-Marjumiid Biomere extinction was observed in China, Australia, and Sweden (Saltzman et al., 2000; Ahlberg et al., 2009). All three late Cambrian extinctions have been noted to be associated with globally correlative carbon isotope excursions (Ripperdan et

* Corresponding author at: Department of Earth Sciences, University College London, London WC1E 6BT, UK.
E-mail address: imchenxi@gmail.com (X. Chen).

https://doi.org/10.1016/j.chemgeo.2023.121456
Received 13 January 2022; Received in revised form 10 March 2023; Accepted 29 March 2023
0009-2541/© 20XX

al., 1992; Saltzman et al., 2011, 2015), confirming their global origins. While the two earlier late Cambrian extinctions are related to the SPICE Event (Steptoean Positive Carbon Isotope Excursion, Saltzman et al., 2000), the last one is related to the TOCE Event (Top Of Cambrian Excursion, Buggisch et al., 2003; Zhu et al., 2006; Peng et al., 2012; Zhu et al., 2021), a negative carbon isotope anomaly that has two synonyms (Zhu et al., 2021): HERB (HEllnmaria–Red Tops Boundary, Ripperdan, 2002; Landing et al., 2020) and SNICE (Sunwaptan Negative Isotope Carbon Excursion, Sial et al., 2013). As with other end-of-biomere extinctions, multiple triggers have been proposed (Westrop and Ludvigsen, 1987; Loch et al., 1993; Runkel et al., 2010), although no clear consensus exists over the cause of either the terminal Cambrian extinction or the TOCE. However, changes in ocean redox conditions may have been a key factor linking those biotic and abiotic events.

In the last decade, uranium isotope ratios (reported as $\delta^{238}U$ values, the per mil variation of $^{238}U/^{235}U$ compared to the standard NBL CRM-145), have been used as a novel ocean redox proxy to investigate relationships between environmental and evolutionary crises (e.g., Dahl et al., 2014; Lau et al., 2016, 2017; Jost et al., 2017; White et al., 2018; Clarkson et al., 2018; Zhang et al., 2019, 2020; del Rey et al., 2020). The redox sensitivity of $\delta^{238}U$ is due to the exchange between the common U species, U(VI) vs. U(IV), and associated U isotope fractionation. In the modern ocean, dissolved U exists as the oxidized U(VI) species in stable uranyl bicarbonate complexes and has a long oceanic residence time (ca. 400 kyr) relative to the ocean mixing time (1–2 kyr). Consequently, its concentration and isotope composition ($\delta^{238}U$) are homogeneously distributed in open-ocean seawater (OSW) (Andersen et al., 2016). While the dissolved riverine U load is the main ocean input, removal may occur as either the oxidized U(VI) or reduced U(IV) species. The largest U sink is U uptake into reducing sediments, where U(VI) is reduced to the largely immobile U(IV) species with a preference for the heavier ^{238}U isotope due to nuclear volume effects (Stirling et al., 2007; Weyer et al., 2008). Although U reduction occurs at or below a redox potential close to that for Fe(III) reduction (i.e., less reducing than 'sulfidic anoxia' or 'euxinia'), and primarily at or below the sediment-water interface (Morford et al., 2005), the observed $^{238}U/^{235}U$ fractionation between sediment and open-ocean seawater ($\Delta_{sed-OSW}$), is greatest under persistently sulfidic bottom waters in semi-restricted basins in modern environments (e.g., Andersen et al., 2014; Cole et al., 2020). Along continental margins, U removal occurs in productive regions under a range of different and 'intermediate' reducing conditions from low-O_2 suboxic[1] to intermittently anoxic conditions (Dunk et al., 2002). Compared with the semi-restricted euxinic U sink, the intermediate reducing sink is associated with only minor expressed $\Delta_{sed-OSW}$, on average (contra: Lau et al., 2022), due to various reasons. Firstly, when reductive U removal occurs within sediments beneath suboxic bottom waters, the expressed $\Delta_{sed-OSW}$ can be lowered due to diffusion limitation on the U supply (Weyer et al., 2008; Andersen et al., 2014; Lau et al., 2020). Secondly, both spatial and temporal variations of oxygen minimum zones (OMZs) may lead to non-steady state U uptake and mute the expressed $\Delta_{sed-OSW}$ (Weyer et al., 2008; Andersen et al., 2016; He et al., 2021; Bruggmann et al., 2022). Thirdly, particulate non-lithogenic uranium (PNU, Zheng et al., 2002), i.e., organic-matter-related U, can contribute significantly to total authigenic U when the bottom water has low dissolved oxygen content (< 25 μM, Zheng et al., 2002). Because PNU is likely depleted in ^{238}U (Holmden et al., 2015; Hinojosa et al., 2016; Abshire et al., 2020), its mixing with U uptake in situ within the sediments, enriched in ^{238}U, can mute the total expressed $\Delta_{sed-OSW}$. In contrast, the U sinks of U(VI) species are smaller than the U(IV) species U sinks (Dunk et al., 2002) and generally associated with smaller U isotope fractionation, but towards lighter isotope compositions (e.g., Fe—Mn nodules have $^{238}U/^{235}U$ that are ~0.2‰ lower than seawater; Goto et al., 2014). A larger U sink is the U(VI) uptake into carbonates, both via biotic or abiotic pathways. Pelagic carbonates show negative $\Delta_{sed-OSW}$ of ca. −0.15‰ (Clarkson et al., 2020), whereas the majority of shallow water carbonates display positive $\Delta_{sed-OSW}$ with an average of ca. +0.25‰ (Romaniello et al., 2013; Chen et al., 2018; Tissot et al., 2018; Lau et al., 2022). Negative $\Delta_{sed-OSW}$ values may derive from effects of U adsorption and/or organic matter (Clarkson et al., 2020, 2021), while positive $\Delta_{sed-OSW}$ values are often attributed to U(IV) incorporation in carbonate cements under reducing porewater conditions. Because modern carbonates deposited under oxic conditions show limited U isotope fractionation, marine carbonates are the favored geological archive for estimating the $\delta^{238}U_{OSW}$ in the past.

The global redox sensitivity of the uranium isotope proxy relates to changing OSW $\delta^{238}U$ values due to the mass-weighted isotope fractionation of the burial flux ($\delta^{238}U_{OSW} = \delta^{238}U_{input} - \sum\Delta_i f_i$, f_i is the proportion for each burial flux) compared to the input. Consequently, geological records of negative $\delta^{238}U$ excursions have been taken to indicate expansion of euxinia (Cole et al., 2020), even though both the modern carbonate and intermediate reducing fluxes contribute a large proportion of the total U sink today compared to euxinic semi-restricted basins (Dunk et al., 2002; Andersen et al., 2016, 2017; Cole et al., 2020). We argue here that the recovery phase of a negative $\delta^{238}U$ excursion could relate to expansion of the intermediate reducing sink, rather than the oxic sink, at the expense of the euxinic sink.

This study presents uranium and carbon isotope profiles and metal concentrations of marine limestones spanning the full TOCE interval at the Wa'ergang section in South China, in order to study the coupling of oceanic redox conditions and the global carbon cycle during the late Cambrian, with implications for improved understanding of the terminal Cambrian extinction event.

2. Materials and methods

The Wa'ergang section is situated in Taoyuan County, western Hunan Province, China. It is located on the southeastern margin of the Yangtze Platform (Fig. 1B). At the end of the Cambrian Period, the Yangtze plate was located on the northern margin of the Gondwana continent. The middle to upper Cambrian strata were continuously deposited in the studied area, and are mainly composed of richly fossiliferous carbonate rocks. A total of 32 dark-gray packstone samples spanning the top Cambrian TOCE Event were collected from the upper part of the Shenjiawan Formation at the Wa'ergang section. The upper Shenjiawan Formation is composed of medium- to thick- bedded packstone with minor siliciclastic content and occasional intercalations of marlstone, and has no systematic lithology changes (Mei et al., 2019). It was deposited in the middle carbonate ramp (Mei et al., 2019) or the outer slope (Li et al., 2017) which should have a good connection to the open ocean because of the occurrences of a rich assemblage of conodonts and trilobites used for intercontinental stratigraphic correlation (Peng et al., 2012, 2014; Bagnoli et al., 2017; Dong and Zhang, 2017). Our sampling was interrupted by a possibly allochthonous massive carbonate debris bed (~3 m) with slump folds, and this bed marks the approximate boundary between the *Eoconodontus* and *Cordylodus proavus* conodont zones (Bagnoli et al., 2017) and also the end-Ptychaspid Biomere extinction horizon (see section 4.3 for more details). The Wa'ergang section above this bed is not as continuous as below, and so previous biostratigraphic (Bagnoli et al., 2017) and carbon isotope chemostratigraphic (Li et al., 2017) studies also stopped around this level.

Fine-grained, micritic limestones without secondary veins and recrystallization were finely powdered. 50–150 μg powder of each sample was reacted with phosphoric acid at 70 °C in a Kiel IV carbonate

[1] We choose "suboxic" to describe the depositional environments with low-O_2 (without specific upper and lower limits of dissolved O_2) bottom waters, because "hypoxic" (used by Andersen et al., 2017) is for "physiological regime" (Tyson and Pearson, 1991) and its definition depends on the specific organism. All the terms for redox conditions (oxic, suboxic, non-sulfidic anoxic, intermediate redox, sulfidic, euxinic) refer to the bottom waters unless additional specifications.

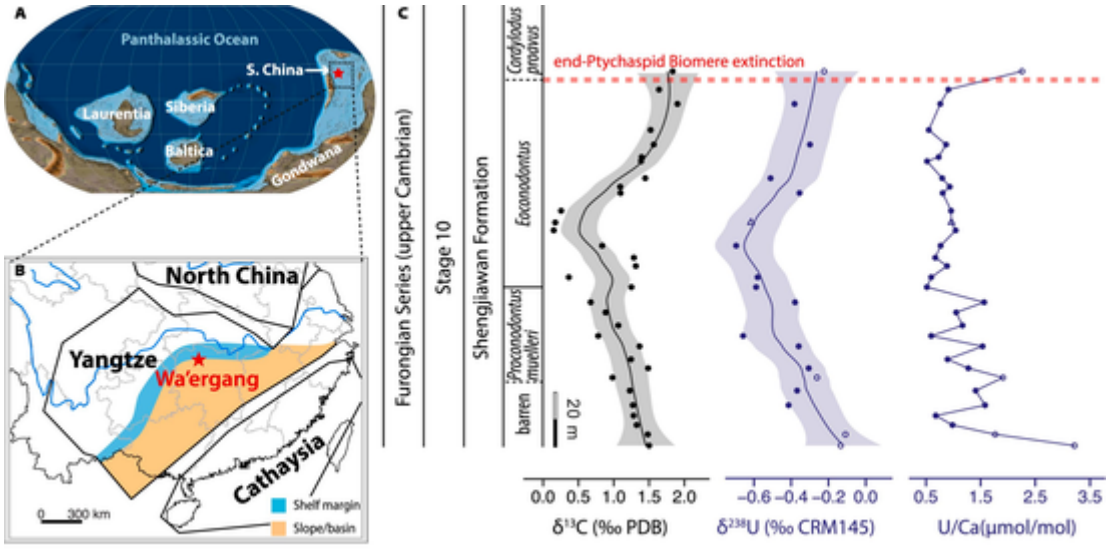

Fig. 1. A: Paleogeographic map showing South China and other paleocontinents during the late Cambrian (Scotese, 2021). The red star marks Wa'ergang section. B: Simplified geological map of South China and the location of Wa'ergang section on the southeastern margin of the Yangtze plate. C: Chemostratigraphic data (carbon and uranium isotope compositions) of late Cambrian succession from Wa'ergang section in Taoyuan County, western Hunan Province, China. The $\delta^{238}U$ data possibly being affected by dolomitization or reducing porewater are denoted by a triangle and open circles, respectively. The $\delta^{238}U$ data are corrected for detrital U contributions. Curves of $\delta^{238}U$ and $\delta^{13}C$ are smoothed by LOESS fitting with shaded 95% confidence intervals. A red dashed line right below a carbonate debris bed marks the boundary between the *Eoconodontus* and *Cordylodus proavus* conodont zones (Bagnoli et al., 2017), and this biozone boundary corresponds to the rising limb of the TOCE (Landing et al., 2011; Saltzman et al., 2015; Li et al., 2017; Azmy, 2019) and the terminal Cambrian end-Ptychaspid Biomere extinction event (Palmer, 1984; Landing et al., 2011). (For interpretation of the references to colour in this figure legend, the reader is referred to the web version of this article.)

device, and the CO_2 generated was analyzed on a MAT 253 mass spectrometer in the Nanjing Institute of Geology and Palaeontology, Chinese Academy of Sciences. Both $\delta^{13}C$ and $\delta^{18}O$ values are reported relative to the V-PDB. The long-term external reproducibilities of $\delta^{13}C$ and $\delta^{18}O$ analyses are ±0.04‰ and ±0.08‰, respectively (1 SD, 600 replicates of the laboratory standard GBW-04405 over one year). Metal concentration and U isotope analyses for 18 out of 32 samples were carried out using an ELEMENT XR ICP-MS (Nanjing University) and NEPTUNE Plus MC-ICP-MS (Nanjing Normal University), respectively. Samples (~100 mg) were leached by agitation for 4 to 12 h in 1 M HCl at room temperature, until no further effervescence was observed (Lau et al., 2016; Zhang et al., 2018). The sample supernatant was separated from the remaining residue. A small aliquot was taken and diluted 500-fold for each sample prior to the metal analyses. Rhodium (Rh) was added as internal standard for analyses (samples and standards). Concentration of each metal was calculated by comparison of the ^{103}Rh-normalized intensity of a sample with that of an artificial standard with high Ca and Mg contents similar to carbonates. The remaining sample was spiked with the IRMM-3636 ^{236}U—^{233}U double spike, aiming for a $^{236}U/^{235}U$ ratio of ~4 before preparation for U purification. The U purification from matrix elements were done using RE resin following published protocols used to successfully separate U from a range different matrix including carbonates (Bura-Nakić et al., 2018, 2020; Clarkson et al., 2020) and subsequently dissolved in 2% (*v*/v) HCl aiming for ~50 ppb U for mass spectrometric measurements. Full procedural blanks were <0.1 ng U, negligible to the sample sizes measured. Uranium isotope measurements were performed in a static collection with 10^{11} Ω resistors on all Faraday cups. Corrections of ^{238}U and ^{235}U impurities (from IRMM-3636), tailing, hydrate formation and mass bias corrections were carried out as described by Andersen et al. (2016). The $\delta^{238}U$ values were measured relative to the NBL CRM-145 standard. The internal precisions (2 SE) on measured $\delta^{238}U$ values are better than ±0.05‰ for all samples. Repeated measurements of the in-house CZ-1 uraninite standard gave $\delta^{238}U = -0.04 \pm 0.06$‰ (2 SD, 45 replicates over two years), in excellent agreement with the obtained values for the same standard from different laboratories with similar analytical set-ups (e.g., Stirling et al., 2007; Andersen et al., 2014, 2016; Bura-Nakić et al., 2018; Clarkson et al., 2020). Further, analyses of the IAPSO seawater gave $\delta^{238}U$ −0.38 ± 0.04‰ (2 SD, $n = 3$) within error of other determinations of this standard (Holmden et al., 2015).

3. Results

The $\delta^{13}C$ values from Wa'ergang section range between +0.15‰ and +2.43‰, and the $\delta^{18}O$ values lie within a narrow range (−10.2 to −8.8‰). The $\delta^{13}C$ profile exhibits a negative excursion in the middle of the section (Fig. 1C). There is no observed covariation between $\delta^{18}C$ versus $\delta^{18}O$ or Mn/Sr (Fig. 2A, B).

The $\delta^{238}U$ data ranges between −0.66‰ and −0.14‰ and shows a depth profile that mimics the $\delta^{13}C$ trend, with a near synchronous negative excursion. Values decrease from −0.14‰ to a nadir of −0.66‰ in the middle, and then return to near initial values (−0.23‰) at the end of the TOCE Event (Fig. 1C). The Ca-normalized U concentration (U/Ca, μmol/mol) ranges between 0.52 and 3.22 (Fig. 1C, 2D). The highest U/Ca ratios are observed at the very beginning and end of the depth profile, whereby the four samples with the highest U/Ca ratios also exhibit the highest $\delta^{238}U$ values. The U/Ca ratios, excluding those four samples, distribute in two groups clustering around 0.8 and 1.5, respectively (Fig. 2D), and show weak correlation with $\delta^{238}U$ values largely due to U/Ca ratios clustering around 1.5. There is no correlation with $\delta^{238}U$ values for the other samples having U/Ca ratios clustering around 0.8, and the range and trend of $\delta^{238}U$ curve exhibited by these samples remains the same as all the samples. The U/Al (ppm/ppm) ratios in the carbonate leachates range from 1.43×10^{-4} to 1.54×10^{-3}. Neither U contents nor U isotope compositions covary with Al concentrations (with correlation coefficients $R^2 < 0.06$ and *p*-values > 0.33).

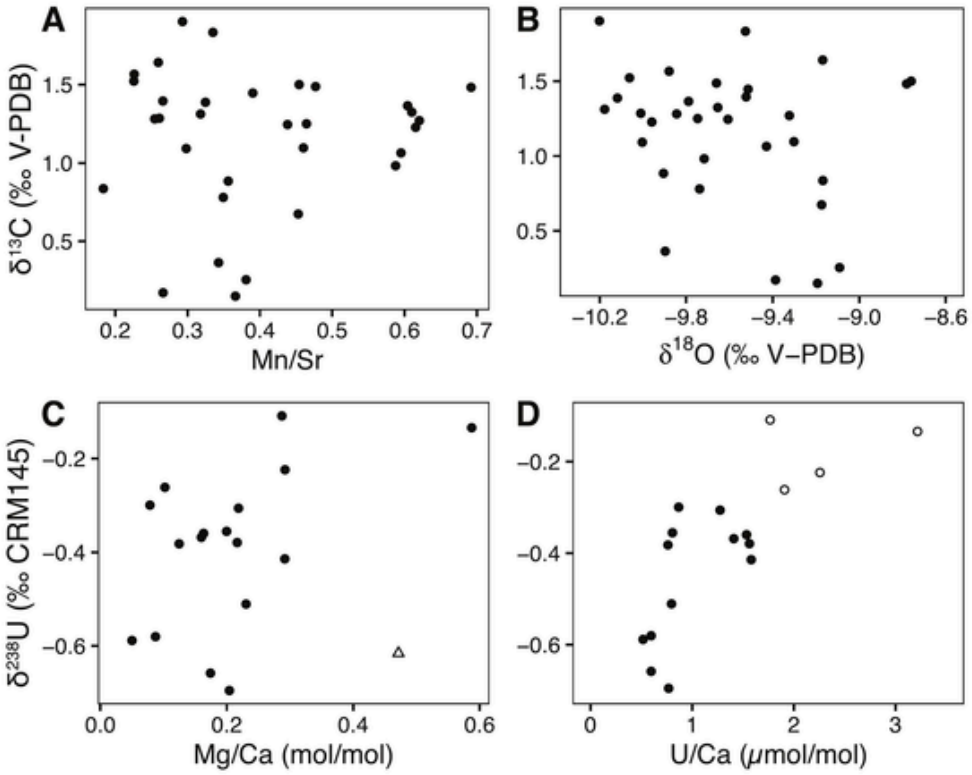

Fig. 2. Cross plots of $\delta^{13}C$ vs. proxies for diagenetic alteration (A: Mn/Sr ratio, B: $\delta^{18}O$), and $\delta^{238}U$ vs. proxies for dolomitization (shift $\delta^{238}U$ to lower values, C: Mg/Ca molar ratio) and reducing porewater (shift $\delta^{238}U$ to higher values, D: U/Ca) in limestone samples from Wa'ergang section. The data possibly being affected by dolomitization or reducing porewater are denoted by a triangle (low $\delta^{238}U$ and high Mg/Ca) and open circles (high $\delta^{238}U$ and high U/Ca), respectively.

4. Discussion

4.1. Assessment of the isotope data

Before interpreting the data in terms of paleoenvironment, it is particularly important to demonstrate that measured data show primary marine signatures and have not been significantly altered by various syngenetic, diagenetic or mixing effects.

Diagenetic alteration of carbonates, by interaction with meteoric waters, tends to deplete Sr and ^{18}O but enrich Mn. Because carbon is a major element in carbonates but is less abundant in meteoric waters, its isotope composition is less susceptible to alteration in comparison to Sr and O isotopes. Limestones with Mn/Sr ratios below 10 have been proposed to most likely preserve primary $\delta^{13}C$ values (Kaufman and Knoll, 1995). In our dataset, Mn/Sr ratios are all lower than 0.7, which is even lower than a proposed upper limit of 2 for preserving primary Sr isotope compositions (Kaufman and Knoll, 1995). Moreover, neither $\delta^{18}O$ nor Mn/Sr, as diagenetic proxies, vary systematically with changes in $\delta^{13}C$ ($R^2 < 0.06$ and p-values > 0.19), which strongly supports use of these carbon isotope data for interpreting the paleoceanic environment.

Prior to using carbonate $\delta^{238}U$ as estimates for $\delta^{238}U_{OSW}$, it is also imperative to address the potential effects of detrital contribution, as well as syngenetic or diagenetic effects. In terms of detrital contribution, the Al content in carbonate leachates may be related to trace levels of detrital siliciclastic rock components that may dissolve during the leaching (e.g., Clarkson et al., 2020) and can therefore be used to assess siliciclastic contamination of the leachates. Assuming that the Al is solely related to the detrital siliciclastic contribution, it is possible to correct the bulk $\delta^{238}U$ values for this by mass balance, based on assumptions about the U/Al and $\delta^{238}U$ of this phase. Assuming U/Al $= 3.5 \times 10^{-5}$ (ppm/ppm; McLennan, 2001) and $\delta^{238}U = -0.3‰$ (Andersen et al., 2014) for the detrital contribution, the magnitude of $\delta^{238}U$ correction would be $< 0.072‰$, which suggests that any influence from detrital U on these limestone leachates is negligible. Similarly, Clarkson et al. (2020) performed leaching experiments on carbonates using different leaching reagents, which revealed no bias in the obtained $\delta^{238}U$ using 1 N HCl compared to a range of other milder leaching methods.

There are several syngenetic or diagenetic effects that may affect carbonate $\delta^{238}U$. Carbonate $\delta^{238}U$ values can decrease during dolomitization, especially when molar Mg/Ca ratios exceed ca. 0.5 (Romaniello et al., 2013). However, data from upper Jurassic carbonates do not show any correlation between the degree of dolomitization (Mg/Ca) and $\delta^{238}U$ values (Herrmann et al., 2018), which is also true for our samples ($R^2 = 0.10$, p-value $= 0.21$, and see Fig. 2C). Furthermore, our samples with low $\delta^{238}U$ values ($< -0.6‰$) generally exhibit low Mg/Ca molar ratios (< 0.21), instead of high ratios, except for one sample with a Mg/Ca molar ratio of 0.47 (denoted by a triangle in Fig. 1C and Fig. 2C). In contrast, the authigenic uptake of additional U under reducing conditions can shift $\delta^{238}U$ to higher values. This effect is likely to result dominantly from uptake of reduced U into carbonate cements under reducing pore-water conditions (e.g., Romaniello et al., 2013; Clarkson et al., 2021). It is striking that the four samples with the highest $\delta^{238}U$ values also have the highest U contents (see Fig. 2D). This suggests that they may have been affected by authigenic uptake of U under reducing conditions, analogous to modern Bahamian carbonates (Romaniello et al., 2013). In Eocene carbonate samples, Clarkson et al. (2021) did observe the effect of reduced U uptake and higher $\delta^{238}U$ with increasing U/Ca, whereby the increase initiated at > 0.125 (μmol/mol) in those samples. While the exact U/Ca threshold in Clarkson et al. (2021) cannot be used in our case due to different oceanographic settings and ocean U budgets, we argue that these four U-rich samples, towards the base and top of the depth profile, might record higher $\delta^{238}U$ than contemporaneous seawater. For the remaining samples with U/

Ca < 1.6, there is no obvious trend of increasing U concentration with high $\delta^{238}U$ (Fig. 2D) and so their measured $\delta^{238}U$ values are considered likely to reflect near seawater $\delta^{238}U$ at the time of carbonate formation.

4.2. The TOCE event: a global negative carbon isotope excursion

The negative $\delta^{13}C$ TOCE excursion has been well-documented in nearly all late Cambrian paleocontinents, including organic carbon isotope profiles in Baltica, and carbonate carbon isotope profiles in western Laurentia, northeastern Laurentia, Precordillera terrane, Siberia, Australia, Tarim, North China and South China (Miller et al., 2015; Azmy, 2019; Landing et al., 2020; Zhu et al., 2021). The amplitude of this $\delta^{13}C$ excursion ranges between −0.5‰ and −4‰. The nadir of TOCE consistently occurs within the lower part of the *Eoconodontus* Zone in most of the aforementioned paleocontinents with sections having well-established biozones (Landing et al., 2011; Azmy, 2019; Landing et al., 2020). Our data from Wa'ergang section show that the onset of the full TOCE Event lies within the *Proconodontus muelleri* Zone (Fig. 1), which is also true for Black Mountain in Australia (Ripperdan et al., 1992) and Sneakover Pass in Utah, USA (Miller et al., 2015). The intercontinentally correlative TOCE excursion implies a perturbation of the global carbon cycle.

There is still no clear consensus on the cause of TOCE, but it may be linked to sea-level changes. The association between the $\delta^{13}C$ minimum of TOCE and a regression event is evidenced from disconformities and detailed sequence stratigraphic analysis on various paleocontinents, including Australia (Ripperdan et al., 1992), North China (Ripperdan et al., 1993) and Laurentia (Miller et al., 2015). Ripperdan (2002) proposed that weathering of 'old carbon' on formerly productive platforms provided the source of isotopically light carbon. However, carbonate was deposited in broad epeiric/marginal seas throughout the late Cambrian (Landing, 2011). Therefore, the net effect of enhanced weathering would have resulted in an input of isotopically heavy rather than light carbon. We suggest that the TOCE Event could have been driven by changes to carbon sinks rather than sources (see detailed discussions in section 4.4 and 4.5).

4.3. Positive carbon and uranium isotope shifts and the terminal Cambrian extinction

The late Cambrian (Furongian Series) records three extinction events at the top of the Marjumiid, Pterocephaliid, and Ptychaspid biomeres, respectively (Palmer, 1984). The youngest one, the end-Ptychaspid Biomere extinction, coincides precisely with the *Eoconodontus–Cordylodus proavus* conodont Zone boundary (Palmer, 1984; Landing et al., 2011). This biostratigraphic level corresponds to the rising limb of the TOCE, i.e., a $\delta^{13}C$ positive shift following the TOCE nadir (Landing et al., 2011; Saltzman et al., 2015; Li et al., 2017; Azmy, 2019), as well as a coeval $\delta^{238}U$ positive shift indicating oxygenation.

Generally, there is evidence against sea-level changes as the direct 'killing mechanism' of the late Cambrian end-of-biomere extinctions: 1) The lithological changes associated with all three end-of-biomere extinctions are not uniform in different locations, and are usually minimal, although obvious faunal turnovers are similar. 2) Well-defined continent-wide regressions occurred *within* the Pterocephaliid and Ptychaspid biomeres without obvious faunal effects (Palmer, 1984; Loch et al., 1993; Taylor, 2006). Specifically, the link between sea-level (and/or climate) changes and the end-Ptychaspid extinction is highly controversial (Westrop and Ludvigsen, 1987, cf. comments by Loch et al., 1993 and Taylor, 2006; Runkel et al., 2010, cf. comments by Landing, 2011).

In contrast, positive $\delta^{13}C$ excursions are strongly related with recurring extinctions from the late Cambrian Furongian Stage to Early Ordovician Tremadocian Stage, providing evidence of periodic expansions of anoxia delaying further animal diversification (Saltzman et al., 1995, 2011, 2015). Coincidence of positive $\delta^{34}S$ shifts at the tops of Marjumiid (Gill et al., 2011) and Symphysurinid (Saltzman et al., 2015) biomeres, and a negative $\delta^{238}U$ shift at the top of the Marjumiid biomere (equivalent to the onset of SPICE, Dahl et al., 2014), provide further evidence for anoxia. However, there has been no strong evidence for anoxia linked with all the other biomeres. Moreover, a negative shift (end-Marjumiid, Dahl et al., 2014), positive shift (end-Ptychaspid, this study), and fluctuation (end-Pterocephaliid, Dahl et al., 2014) of $\delta^{238}U$ have all been observed during the end-of-biomere extinctions, which appears to weaken the proposed link between end-of-biomere extinctions and anoxia.

4.3.1. Relationships between $\delta^{13}C$ and $\delta^{238}U$

Negative $\delta^{238}U$ shifts are observed to be associated with both positive and negative $\delta^{13}C$ shifts. The former situation was observed from early and late Cambrian (Dahl et al., 2014), late Silurian (del Rey et al., 2020), Late Devonian (White et al., 2018), and mid-Cretaceous (Clarkson et al., 2018) successions, which is commonly explained by enhanced organic carbon (^{13}C-depleted) burial due to expansion of anoxia. The latter situation was observed from Cryogenian (Lau et al., 2017), end-Permian to earliest Triassic (Zhang et al., 2020), Early Triassic (Zhang et al., 2019), and Triassic/Jurassic boundary (Jost et al., 2017) successions, which has been attributed to anoxia caused by the release of isotopically light carbon sourced from volcanic degassing and/or remineralization of sedimentary or oceanic organic carbon reservoirs.

Positive $\delta^{238}U$ shifts follow negative shifts through most $\delta^{238}U$ 'excursions' (contra: Lau et al., 2017), indicating the waning of anoxia after a perturbation. During a positive $\delta^{13}C$ excursion, a positive $\delta^{238}U$ shift usually corresponds to the recovery/falling limb of the $\delta^{13}C$ excursion (e.g., del Rey et al., 2020; White et al., 2018; Lau et al., 2016; Clarkson et al., 2018; contra: positive $\delta^{238}U$ shift prior to $\delta^{13}C$ recovery in Dahl et al., 2014). However, during a negative $\delta^{13}C$ excursion, a positive $\delta^{238}U$ shift can simply correspond to the recovery/rising limb of the $\delta^{13}C$ excursion (Zhang et al., 2020), or lag behind the beginning of $\delta^{13}C$ recovery due to sustained anoxia (Jost et al., 2017), or be absent due to even more prolonged anoxia (Lau et al., 2017).

Nearly synchronous negative $\delta^{13}C$ and $\delta^{238}U$ excursions, including both falling and rising limbs, as we observe for TOCE, are therefore evidently rare (e.g., Zhang et al., 2020). Besides, all the aforementioned cases with negative shifts of both $\delta^{13}C$ and $\delta^{238}U$ are likely related to release of ^{12}C-enriched carbon causing warming and anoxia (Lau et al., 2017; Jost et al., 2017; Zhang et al., 2019, 2020), while the falling limb of TOCE has been linked to sea-level fall and therefore cooling without evidence for a significant perturbation in carbon input. Almost all the aforementioned negative $\delta^{238}U$ shifts are also accompanied by the deleterious effects of anoxia on animals (contra: Tostevin et al., 2019), but the terminal Cambrian extinction is above the nadir of TOCE and coincident with a positive $\delta^{238}U$ shift indicating oxygenation. These unusual features of the TOCE Event could be explained by significant abiotic and biotic roles played by intermediate reducing conditions, as discussed in the following three sub-sections.

4.4. Changing intermediate reducing settings conducive to positive $\delta^{13}C$ vs. $\delta^{238}U$ covariation

The seawater $\delta^{13}C$ value is proportional to the relative fraction of carbon buried as organic matter when there are no significant changes in the sources. In modern oceans, ~80% of organic carbon is buried in deltaic sediments and is mainly of terrestrial origin (Schlesinger and Melack, 1981; Berner, 1982). The deltaic sink of the late Cambrian would have been significantly reduced because of the lack of land plants. If we omit this sink, the euxinic organic C sink comprises only < 5% of the total, whereas about half of organic C burial occurs in intermediate reducing settings (Berner, 1982). By comparison, U isotopic

fractionation is most significant in euxinic settings, while muted in intermediate reducing settings (see section 1 and following discussions). Therefore, $\delta^{238}U$ is a proxy for the extent of persistent sulfidic anoxia, and is highly sensitive at its higher end, but becomes insensitive at its lower end, because a disproportionately large fraction (~24%) of reduced U is buried in modern euxinic settings even though they account for only <0.1% of global sea-floor area (Dunk et al., 2002; Andersen et al., 2016). Although a significant change in $\delta^{238}U$ still requires a change in the areal extent of euxinia, with a range starting close to 0 (see Fig. 3), larger concurrent changes to C and U burial in intermediate reducing settings (vs. deltaic sediments, as proposed by Dahl et al., 2014) can lead to strong positive coupling of $\delta^{13}C$ and $\delta^{238}U$, as observed throughout the TOCE Event. Specifically, an expansion of intermediately reducing settings, with a required contraction of euxinic settings, would result in a positive shift in $\delta^{238}U$. Because intermediate reducing settings are associated with a large organic carbon burial flux, a positive shift in $\delta^{13}C$ is also expected. Conversely, a decrease in intermediately reducing settings (with an increase in euxinic sediments) would result in a negative shift in $\delta^{238}U$ and potentially a negative shift in $\delta^{13}C$ (see Fig. 3A and section 4.5 for further explanations of this scenario).

Redox reconstruction of a continental margin transect provides evidence for the early Cambrian establishment of modern-type OMZs dominated by ferruginous conditions and surrounded by oxic waters (Guilbaud et al., 2018). The persistence of small carbonaceous fossils within the Baltic OMZ suggests that the OMZ oscillated between oxic and ferruginous conditions (Guilbaud et al., 2018). Such specific and dynamic oceanic redox conditions are likely to lead to muted expressed average $\Delta_{sed-OSW}$ (Weyer et al., 2008; Cole et al., 2020; He et al., 2021; Bruggmann et al., 2022). The occurrence of such dynamic OMZs could have increased in the late Cambrian due to the progressive warming that occurred since the early Cambrian (Frakes et al., 1992), and therefore their impacts on U and C budgets could have also been enhanced. The sea-level controlled changes in intersection areas of OMZs and continental margins (Lau et al., 2016) would have enhanced the coupling of $\delta^{13}C$ and $\delta^{238}U$.

During the late Cambrian, low atmospheric pO_2 (ca. 50% present atmospheric level, Krause et al., 2018), together with low O_2 water solubility in a typical greenhouse climate (Berner, 1990; Frakes et al., 1992; Trotter et al., 2008; Landing, 2012), would have suppressed the dissolved-oxygen level in the surface ocean seawater. Furthermore, there is no unambiguous evidence for late Cambrian polar ice caps, and thus modern-like thermohaline circulation ventilating the deep ocean may not have existed then (Landing, 2012). Saline seawater with low O_2 concentration from lower latitude marginal seas may have contributed to the deep ocean seawater, leading to halothermal instead of thermohaline circulation (Brass et al., 1982; Railsback et al., 1990). Therefore, redox conditions with suboxic bottom waters and underlying anoxic sediments could have been more expansive in both shallow epeiric/marginal waters and deep open oceans, rather than mainly confined within highly productive continental shelves like today (ca. 6% of modern sea-floor area, Andersen et al., 2016). It is noteworthy that eukaryote-dominated "aquatic bioturbation" may have suppressed persistent euxinia and maintained the ventilation of the deep ocean since the early Cambrian (Butterfield, 2018), even when suboxic waters expanded due to physical causes mentioned above. In contrast to the marginal OMZs, such deep ocean suboxic conditions could have been more stable, although the effective $\Delta_{sed-OSW}$ would also have been muted because reductive U removal within the anoxic sediments was diffusion-limited (Weyer et al., 2008; Andersen et al., 2014; Lau et al., 2020).

Under both aforementioned intermediate reducing settings, organic-matter-related PNU may have been high, even in pelagic settings because of higher preservation potential for the 'marine snow' in a

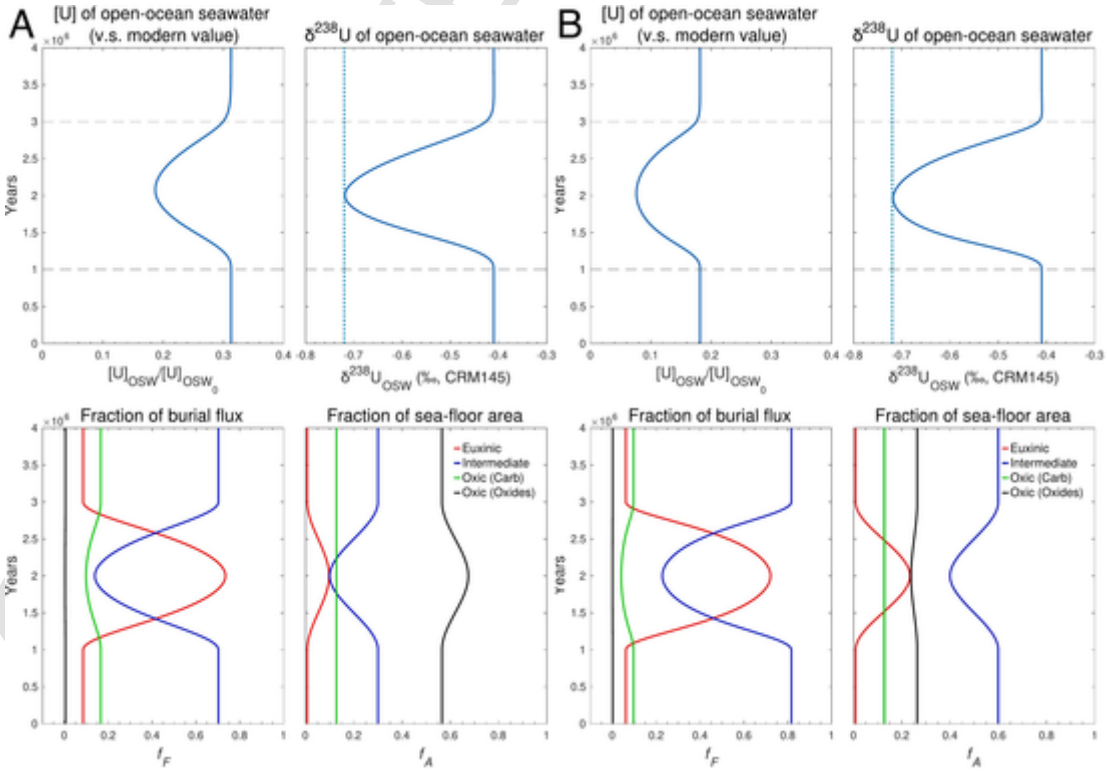

Fig. 3. The results of simple semi-quantitative mass balance modeling for the evolution of open-ocean seawater (OSW) $\delta^{238}U$ under two scenarios of changing intermediate reducing and euxinic areas during the terminal Cambrian. The initial f^{A}_{inter} is 30% and 60% in scenarios A and B, respectively, and it evolves to decrease by 20% in both scenarios. The oxic areal extent of carbonate deposits is held constant. This modeling mainly demonstrates: 1) An obtained $\delta^{238}U_{OSW}$ value could accommodate various combinations of proportions of redox conditions; 2) A scenario with higher f^{A}_{inter} has a smaller oceanic U reservoir; 3) How [U] and $\delta^{238}U$ of OSW respond to changes in negatively correlated f^{A}_{eux} and f^{A}_{inter}, and the magnitude of increase in f^{A}_{eux} could be less than the magnitude of decrease in f^{A}_{inter} (scenario A).

less-oxygenated ocean than today. As PNU is likely depleted in ^{238}U (Holmden et al., 2015; Hinojosa et al., 2016; Abshire et al., 2020), the co-deposition of lighter C and U isotopes, mediated by organic matter, could further enhance the positive coupling of $\delta^{13}C$ and $\delta^{238}U$. However, PNU may be mixed in all U sinks that contain organic matter and is not considered as a separate component in quantitative U isotope mass-balance models.

We utilize a simple semi-quantitative mass balance model to evaluate the impact of intermediate reducing settings on the global U cycle. Firstly, the duration and magnitude of the $\delta^{238}U$ excursion during the TOCE Event have to be estimated. The whole excursion, including both decreasing and rising limbs, spans about two conodont zones, or half of Cambrian Stage 10 (489.5–485.4 Ma), which suggests a duration of ca. 2 Myr. Because the start and end points of the $\delta^{238}U$ dataset have likely been impacted by incorporation of reduced U, we choose the stratigraphically lowest sample with relatively low U/Ca, and use its $\delta^{238}U_{carb}$ value (−0.41‰) as the starting level for $\delta^{238}U_{OSW}$. For the sake of simplification, we consider that the studied interval ends at the same level as indicated by the overall $\delta^{238}U_{carb}$ trend.

In the modern, the intermediate reducing sink of U has a lower burial rate and a smaller average isotope fractionation factor ($\Delta_{inter-OSW} \approx +0.15‰$) than the euxinic sink (cf. typical $\Delta_{eux-OSW}$ is between +0.4‰ and +0.6‰, Andersen et al., 2014; Cole et al., 2020). Combining those two factors, a greater areal fraction of the intermediate reducing settings (f^A_{inter}) at the cost of euxinic settings (f^A_{eux}) would have increased both the ocean U reservoir and the $\delta^{238}U_{OSW}$, and vice versa, as demonstrated in the modeled oceanic U evolution through time in Fig. 3. It is important to note that an obtained $\delta^{238}U_{OSW}$ value could accommodate various combinations of proportions of redox conditions, as demonstrated by modeling scenario A versus B in Fig. 3. A scenario with a higher f^A_{inter} has a smaller oceanic U reservoir. For example, obtaining a $\delta^{238}U_{OSW}$ of −0.41‰, as used as the initial state, scenario B with a higher f^A_{inter} (60%) than scenario A (30%) induces a lower $[U]_{OSW}$ for scenario B than A (18% vs. 31% of modern level for A and B, respectively). Therefore, even if the $\delta^{238}U_{OSW}$ was similar to the modern value, the oceanic U reservoir could have been smaller and probably more sensitive to changes in oceanic redox state during times when intermediate reducing settings were more expansive (scenario B vs. A, or late Cambrian vs. modern).

Obviously, the modeling has some caveats including the definition and choice of set values of the parameters used (listed in Table 1). However, our main purpose here is to illustrate how different changes in the relative proportions of intermediate reducing and euxinic U sinks can drive the same observed shifts in $\delta^{238}U$, and to highlight the importance of the intermediate reducing sink in minimizing the oceanic U reservoir and inducing positive $\delta^{238}U$ shifts. An overall increasing size of the intermediate reducing U sink, including modern-type dynamic OMZ settings and persistently suboxic settings overlying anoxic sediments, should create a higher $\delta^{238}U$ baseline than an ocean dominated by a sustained euxinic sink. Plotting a compilation of available carbonate $\delta^{238}U$ data from late Ediacaran to Cambrian times (Fig. 4) shows, despite considerable variability in the data, a higher $\delta^{238}U$ baseline (reflected in median, mean, and nadirs of negative excursions) during the Cambrian than the Ediacaran. The $\delta^{238}U$ data from this study are consistent with this higher baseline.

Table 1
Parameters used in U mass balance modeling.

Parameter	Value
U concentration[a] and isotope composition[b] in modern open-ocean seawater	3.238 ppb, −0.39‰
Total volume of the ocean	1.37×10^{21} L
Total area of ocean floor	3.61×10^{14} m^2
Modern rate of U output flux and isotope fractionation[b]:	
Euxinic	1.130×10^{-3} g m^{-2} yr^{-1}, +0.42‰
Intermediate reducing	2.088×10^{-4} g m^{-2} yr^{-1}, +0.15‰
Carbonates (oxic)	1.158×10^{-4} g m^{-2} yr^{-1}, 0‰
Metalliferous (oxic)	7.121×10^{-7} g m^{-2} yr^{-1}, −0.25‰
Modern U output flux and isotope fractionation: hydrothermal[b, c]	6×10^6 mol, +0.25‰
Modern total U input flux and isotope composition[b, d]	45×10^6 mol, −0.246‰

[a] Chen et al. (1986).
[b] Based on U output flux and areal fraction of each redox setting estimated by Andersen et al. (2016).
[c] Assume constant values.
[d] Assume steady state of modern marine ^{238}U—^{235}U budget.

4.5. Plausible climatic and oceanic drivers

Unlike most reported cases with covarying negative $\delta^{13}C$ and $\delta^{238}U$ shifts (e.g., Lau et al., 2017; Jost et al., 2017; Zhang et al., 2019, 2020), there is no evidence for either warming or significant injection of isotopically light carbon (e.g., volcanic degassing, oxidization of methane hydrates or DIC pool) during the TOCE Event. On the contrary, as mentioned in section 4.2, there is evidence for sea-level fall and thus cooling associated with the TOCE nadir.

Divergent trends in deep and upper ocean redox conditions in response to cooling have been suggested for the last glacial maximum (LGM, Jaccard and Galbraith, 2012) and end-Ordovician (Bartlett et al., 2018; Pohl et al., 2021) periods. Cooling increases oxygen solubility and oxygenates the upper ocean (<1500 m, Riedinger et al., 2021). However, reduced efficiency in ocean circulation, which would transport less oxygen to depth (i.e., ventilation), and/or slowing down in the degradation of sinking organic matter (i.e., biological pump), could deoxygenate the deep ocean (Sigman et al., 2010; Matsumoto, 2007). Therefore, we prefer scenario A in Fig. 3 as a better fit for the ocean redox changes during the TOCE Event, with a spread of both anoxic (possibly in deep ocean) and oxic areas (possibly in shallower ocean), at the expense of intermediate reducing areas. When the magnitude of a $\delta^{238}U_{OSW}$ negative excursion is a known fixed value, a higher f^A_{inter} baseline requires a larger expansion of euxinia to compensate for the inefficiency of the intermediate reducing sink in burying the heavier ^{238}U isotope during a negative $\delta^{238}U$ shift. As demonstrated in Fig. 3, when the f^A_{inter} evolves to decrease by 20% in both scenarios, scenario A with a smaller initial f^A_{inter} (30%) requires f^A_{eux} to be ca. 10%, whereas scenario B with a larger initial f^A_{inter} (60%) requires f^A_{eux} to be ca. 23%. Importantly, in scenario B, the increase in f^A_{eux} is comparable to the decrease in f^A_{inter}, which is inconsistent with the observed negative $\delta^{13}C$ shift. Considering that the modern deep ocean (water depth > 1500 m) comprises 86% of the total ocean area, the intermediate reducing conditions have to be largely distributed in the deep ocean for scenario B with a higher f^A_{inter} baseline (60%). In contrast, our preferred scenario A, which assumes a lower f^A_{inter} baseline (30%), implies relatively limited distribution of intermediate reducing conditions, probably in areas covered by the oldest and most O_2-deficient bottom seawater and/or related with eastern boundary upwelling and thus high primary productivity. Slower ventilation and/or a more efficient biological pump during cooling would have promoted euxinia in those areas.

Convergent trends in deep and upper ocean redox conditions during a warming/transgressive interval would have increased the extent of both anoxic and intermediate reducing settings, and been reflected by a negative $\delta^{13}C$ vs. $\delta^{238}U$ correlation, such as observed from the onset of the SPICE (Dahl et al., 2014). However, the upper part of the positive $\delta^{13}C$ shift of SPICE is associated with a positive $\delta^{238}U$ shift and a regression (Saltzman et al., 2000; Dahl et al., 2014; Egenhoff et al., 2015), which is explained by increasing deltaic sinks for both C and U

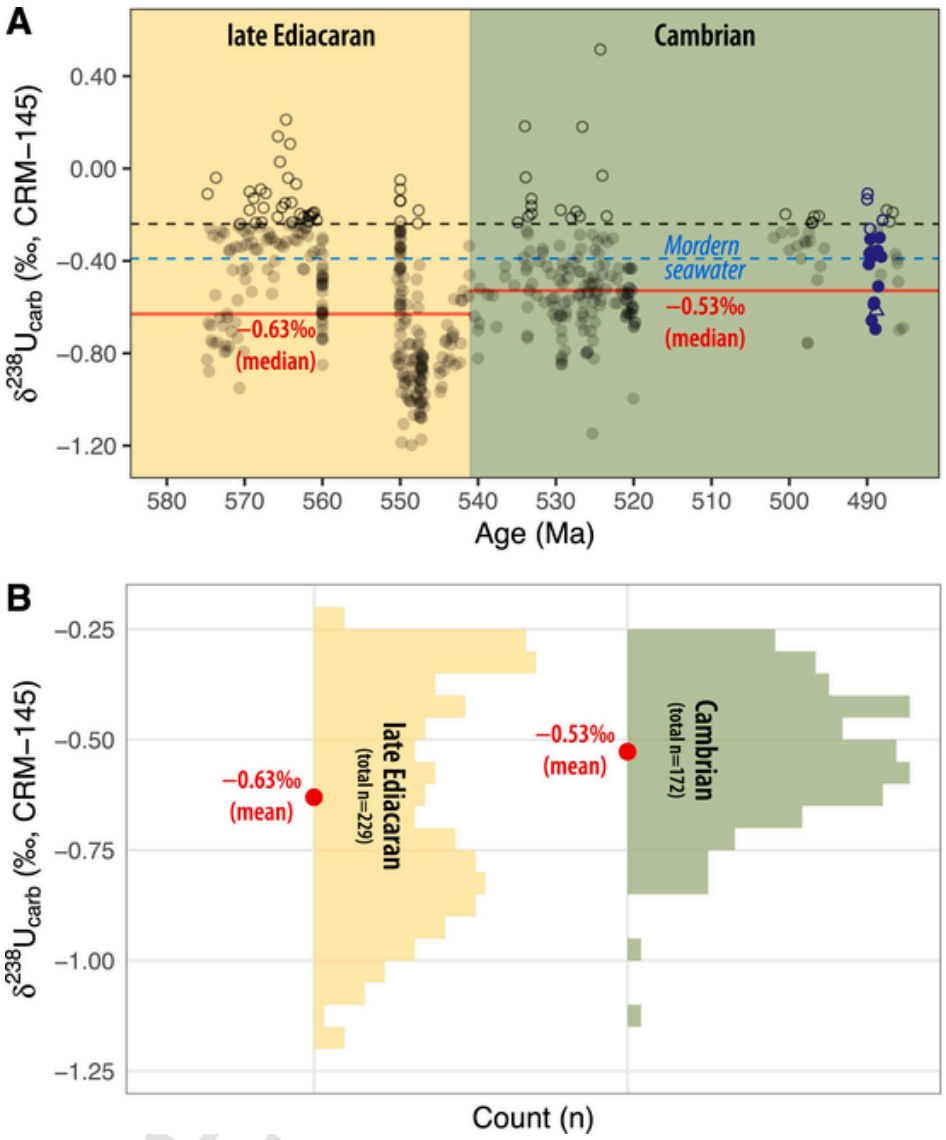

Fig. 4. $\delta^{238}U$ in carbonates from late Ediacaran to Cambrian. A) $\delta^{238}U$ data measured in this study are colored in blue. Gray data points are literature data compiled by Chen et al. (2021). Circles are data greater than the riverine input value (−0.24‰, note that the highest estimate compiled by Andersen et al. (2016) is used as the criteria) marked by the black dashed line. The blue dashed line marks the modern seawater value (−0.39‰, Andersen et al., 2016). The red lines are the medians of late Ediacaran and Cambrian, excluding values higher than the riverine input value. B) Probability distribution plots of $\delta^{238}U$ values of late Ediacaran (yellow, n = 229) and Cambrian (green, n = 172), excluding values higher than the riverine input value. The mean $\delta^{238}U$ value (red dots) increased significantly (a one-sided t-test yields a p-value of 4.4×10^{-7}) from late Ediacaran to Cambrian. (For interpretation of the references to colour in this figure legend, the reader is referred to the web version of this article.)

by Dahl et al. (2014). We propose that it may also have been due to oxygenation of former anoxic areas and increasing intermediate reducing settings that sustained organic carbon burial without preferential burial of heavy U isotopes. It is noteworthy that those positive shifts of both $\delta^{13}C$ and $\delta^{238}U$ start (vs. TOCE: end) with an end-of-biomere extinction, follow an ongoing positive (vs. TOCE: negative) $\delta^{13}C$ shift, and are associated with a regression (vs. TOCE: recovery from regression), while the scenario for the rising limb of TOCE is quite the opposite for all those aspects.

4.6. Implications for the end-of-biomere extinctions

We propose that the shifts to higher values for both $\delta^{13}C$ and $\delta^{238}U$, following nadirs, at the terminal Cambrian extinction level, resulted from an expansion of intermediate reducing settings and a concurrent reduction of euxinic settings. This apparently contradicts the traditional hypothesis that anoxia was the 'killing mechanism' for the end-of-biomere extinctions. An expansion of persistent euxinia would have exterminated both shallow- and deeper-water fauna, and inhibited animal diversification (e.g., end-Permian extinction). However, such a scenario contradicts the observations that: 1) Benthic faunas and/or bioturbation occur in worldwide successions during the SPICE interval encompassing the first and second end-of-biomere extinctions (Wotte and Strauss, 2015; Egenhoff et al., 2015); 2) Abundant epifaunal orthid brachiopods co-occurred with the olenimorphs during the second and third end-of-biomere extinctions (Taylor, 2006); 3) All the end-of-biomere extinctions had both high diversification and high extinction rates (Fortey, 1989), and shoreward extending deeper-water benthos, such as olenid trilobites, show a significant higher survival than endemic shelf taxa (Stitt, 1975; Palmer, 1984; Westrop and Ludvigsen, 1987). By contrast, an expansion of intermediate reducing conditions would remove onshore high-O_2-obligatory incumbents, while giving opportunities to the offshore low-O_2-tolerant fauna (Hallam et al., 1989), such as olenimorphs and brachiopods (Farrell et al., 2011). Moreover, intermediate

reducing conditions may also reinforce evolutionary innovations (Wood and Erwin, 2018). It is noteworthy that the innovation-promoting 'anoxia', with DO < ~0.5 mL/L and/or dynamic redox, used by Wood and Erwin (2018; see section "II. Low-oxygen habitats: ecology and evolution"), is almost equivalent to the 'intermediate reducing' term used herein, rather than to persistent anoxia or euxinia.

Importantly, the loci of reducing conditions are even more pertinent to the extinctions/turnovers than their areal extents. A negative $\delta^{238}U$ shift is observed to *end* with the end-Marjumiid Biomere extinction (Dahl et al., 2014), but obviously *precede* the terminal Cambrian end-Ptychaspid Biomere extinction (this study), respectively, which indicates an expansion of euxinia possibly occurring in the deep ocean for both cases. While no biological effect has been observed for the latter case possibly due to sustained oxic conditions in shallow oceans (similar to the scenario for terminal Ediacaran proposed by Tostevin et al., 2019), the former case may have been associated with invasion of intermediate reducing conditions eliminating animals confined to shelf settings. The later positive shifts of both $\delta^{13}C$ and $\delta^{238}U$ for the latter case is associated with transgression (Miller et al., 2015), and possibly also warming. Both warming and transgression is conducive to upward and landward movements of OMZs (Riedinger et al., 2021). Although the direction of sea-level change at the exact time of the terminal Cambrian extinction is still in dispute (see section 4.3), the OMZ encroachment(s) upon formerly oxygenated nearshore habitats could have been geologically transient and blurred in geological records, but still sufficient to eliminate endemic and introduce immigrant species.

5. Conclusions

Wa'ergang section $\delta^{238}U$ data, spanning an interval that includes the terminal Cambrian extinction event, exhibit a negative excursion parallel to the TOCE carbon isotope event. Negative $\delta^{13}C$ and $\delta^{238}U$ shifts during other events were reported by previous studies, but the recovery phases of these negative excursions are rarely parallel. More significantly, those events are commonly attributed to the release of isotopically light carbon inducing global warming, which is inconsistent with evidence for a regression at the nadir of the TOCE. As with other end-of-biomere extinctions, the terminal Cambrian extinction level is associated with a positive $\delta^{13}C$ shift (i.e., rising limb of the TOCE Event). However, unlike some of the end-of-biomere and many major Phanerozoic extinctions, which were also linked to anoxic events based on S (positive $\delta^{34}S$ shift) and/or U (negative $\delta^{238}U$ shift) isotope data, the terminal Cambrian extinction horizon is associated with a positive $\delta^{238}U$ shift, which is generally considered to indicate ocean oxygenation.

The positive $\delta^{13}C$ vs. $\delta^{238}U$ covariation can be explained by the changing extent of intermediate reducing settings, which are likely to have been widespread during the late Cambrian with low atmospheric pO_2 and a greenhouse climate. A higher $\delta^{238}U$ baseline (mean or median) in Cambrian, compared with late Ediacaran oceans is also consistent with the increasing importance of the intermediate reducing sink.

Coeval negative $\delta^{13}C$ and $\delta^{238}U$ excursions could have been driven by divergent trends in lower and upper ocean redox conditions in response to climate changes. The rising limbs of those isotope excursions, at the terminal Cambrian extinction level, could have resulted from an increase in the intermediate reducing sink for both C and U. An expansion of intermediate reducing settings, rather than anoxic euxinia, is more consistent with the presence of benthic faunas and biogeographical changes associated with not only the terminal Cambrian, but also other end-of-biomere extinctions.

Although a significant shift in the $\delta^{238}U$ value indicates a change in the extent of euxinia, it may co-occur with a change in the extent of intermediate reducing conditions. The loci, rather than merely the extents, of those reducing conditions are particularly pertinent to the biotic effects. Therefore, both positive and negative shifts in $\delta^{238}U$ have been linked with extinction events. Progressive understanding about geochemical proxies and the nature of specific biotic events should be combined to keep testing the proposed cause-and-effect linkage between past environmental changes and biological evolution.

Uncited reference

Declaration of Competing Interest

The authors declare that they have no known competing financial interests or personal relationships that could have appeared to influence the work reported in this paper.

Data availability

Data will be made available on request.

Acknowledgements

This research was supported by Natural Science Foundation of China (41603006, 41661134048) and Strategic Priority Research Program (B) of the Chinese Academy of Sciences (XDB26000000). We thank Shan-Chi Peng and Xue-Jian Zhu (NIGPAS) for guidance on fieldwork; Tao Yang (NJU) for help with ICP-MS; Jing Liu (NIGPAS) for carbon isotope analyses; Qian Liu and Pan Sun (NJU) for their assistance in the chemistry lab. Thomas Algeo and an anonymous reviewer provided perceptive and constructive critical comments on the manuscript, and their input significantly improved the manuscript.

References

Abshire, M.L., Romaniello, S.J., Kuzminov, A.M., Cofrancesco, J., Severmann, S., Riedinger, N., 2020. Uranium isotopes as a proxy for primary depositional redox conditions in organic-rich marine systems. Earth Planet. Sci. Lett. 529, 115878. https://doi.org/10.1016/j.epsl.2019.115878.

Ahlberg, P., Axheimer, N., Babcock, L.E., Eriksson, M.E., Schmitz, B., Terfelt, F., 2009. Cambrian high-resolution biostratigraphy and carbon isotope chemostratigraphy in Scania, Sweden: first record of the SPICE and DICE excursions in Scandinavia. Lethaia 42, 2–16. https://doi.org/10.1111/j.1502-3931.2008.00127.x.

Andersen, M.B., Romaniello, S., Vance, D., Little, S.H., Herdman, R., Lyons, T.W., 2014. A modern framework for the interpretation of $^{238}U/^{235}U$ in studies of ancient ocean redox. Earth Planet. Sci. Lett. 400, 184–194. https://doi.org/10.1016/j.epsl.2014.05.051.

Andersen, M.B., Vance, D., Morford, J.L., Bura-Nakic, E., Breitenbach, S.F.M., Och, L., 2016. Closing in on the marine $^{238}U/^{235}U$ budget. Chem. Geol. 420, 11–22. https://doi.org/10.1016/j.chemgeo.2015.10.041.

Andersen, M.B., Stirling, C.H., Weyer, S., 2017. Uranium isotope fractionation. Rev. Mineral. Geochem. 82, 799–850. https://doi.org/10.2138/rmg.2017.82.19.

Azmy, K., 2019. Carbon-isotope stratigraphy of the uppermost Cambrian in eastern Laurentia: implications for global correlation. Geol. Mag. 156, 759–771. https://doi.org/10.1017/S001675681800002X.

Bagnoli, G., Peng, S., Qi, Y., Wang, C., 2017. Conodonts from the Wa'ergang section, China, a potential GSSP for the uppermost stage of the Cambrian. Res. Paleontol. Stratigr. 123. https://doi.org/10.13130/2039-4942/8003.

Bartlett, R., Elrick, M., Wheeley, J.R., Polyak, V., Desrochers, A., Asmerom, Y., 2018. Abrupt global-ocean anoxia during the Late Ordovician–early Silurian detected using uranium isotopes of marine carbonates. Proc. Natl. Acad. Sci. U. S. A. 115, 5896–5901. https://doi.org/10.1073/pnas.1802438115.

Berner, R.A., 1982. Burial of organic carbon and pyrite sulfur in the modern ocean: Its geochemical and environmental significance. Am. J. Sci. 282, 451–473. https://doi.org/10.2475/ajs.282.4.451.

Berner, R.A., 1990. Atmospheric carbon dioxide levels over Phanerozoic time. Science 249, 1382–1386. https://doi.org/10.1126/science.249.4975.1382.

Brass, G.W., Southam, J.R., Peterson, W.H., 1982. Warm saline bottom water in the ancient ocean. Nature 296, 620. https://doi.org/10.1038/296620a0.

Bruggmann, S., Gilleaudeau, G.J., Romaniello, S.J., Severmann, S., Canfield, D.E., Anbar, A.D., Scholz, F., Frei, R., 2022. Uranium isotope cycling on the highly productive Peruvian margin. Chem. Geol. 590, 120705. https://doi.org/10.1016/j.chemgeo.2021.120705.

Buggisch, W., Keller, M., Lehnert, O., 2003. Carbon isotope record of Late Cambrian to Early Ordovician carbonates of the Argentine Precordillera. Palaeogeogr., Palaeoclimatol. Palaeoecol. 195, 357–373. https://doi.org/10.1016/S0031-0182(03)00365-1.

Bura-Nakić, E., Andersen, M.B., Archer, C., de Souza, G.F., Marguš, M., Vance, D., 2018. Coupled Mo-U abundances and isotopes in a small marine euxinic basin: Constraints on processes in euxinic basins. Geochim. Cosmochim. Acta 222, 212–229. https://

doi.org/10.1016/j.gca.2017.10.023.
Bura-Nakić, E., Sondi, I., Mikac, N., Andersen, M.B., 2020. Investigating the molybdenum and uranium redox proxies in a modern shallow anoxic carbonate rich marine sediment setting of the Malo Jezero (Mljet Lakes, Adriatic Sea). Chem. Geol. 533, 119441. https://doi.org/10.1016/j.chemgeo.2019.119441.
Butterfield, N.J., 2018. Oxygen, animals and aquatic bioturbation: An updated account. Geobiology 16, 3–16. https://doi.org/10.1111/gbi.12267.
Chen, J.H., Edwards, R.L., Wasserburg, G.J., 1986. ^{238}U, ^{234}U and ^{232}Th in seawater. Earth Planet. Sci. Lett. 80, 241–251. https://doi.org/10.1016/0012-821X(86)90108-1.
Chen, X., Romaniello, S.J., Herrmann, A.D., Hardisty, D., Gill, B.C., Anbar, A.D., 2018. Diagenetic effects on uranium isotope fractionation in carbonate sediments from the Bahamas. Geochim. Cosmochim. Acta 237, 294–311. https://doi.org/10.1016/j.gca.2018.06.026.
Chen, X., Tissot, F.L.H., Jansen, M.F., Bekker, A., Liu, C.X., Nie, N.X., Halverson, G.P., Veizer, J., Dauphas, N., 2021. The uranium isotopic record of shales and carbonates through geologic time. Geochim. Cosmochim. Acta 300, 164–191. https://doi.org/10.1016/j.gca.2021.01.040.
Clarkson, M.O., Stirling, C.H., Jenkyns, H.C., Dickson, A.J., Porcelli, D., Moy, C.M., Pogge von Strandmann, P.A.E., Cooke, I.R., Lenton, T.M., 2018. Uranium isotope evidence for two episodes of deoxygenation during Oceanic Anoxic Event 2. Proc. Natl. Acad. Sci. U. S. A. 115, 2918–2923. https://doi.org/10.1073/pnas.1715278115.
Clarkson, M.O., Müsing, K., Andersen, M.B., Vance, D., 2020. Examining pelagic carbonate-rich sediments as an archive for authigenic uranium and molybdenum isotopes using reductive cleaning and leaching experiments. Chem. Geol. 539, 119412. https://doi.org/10.1016/j.chemgeo.2019.119412.
Clarkson, M.O., Lenton, T.M., Andersen, M.B., Bagard, M.-L., Dickson, A.J., Vance, D., 2021. Upper limits on the extent of seafloor anoxia during the PETM from uranium isotopes. Nat. Commun. 12, 399. https://doi.org/10.1038/s41467-020-20486-5.
Cole, D.B., Planavsky, N.J., Longley, M., Böning, P., Wilkes, D., Wang, X., Swanner, E.D., Wittkop, C., Loydell, D.K., Busigny, V., Knudsen, A.C., Sperling, E.A., 2020. Uranium isotope fractionation in non-sulfidic anoxic settings and the global uranium isotope mass balance. Global Biogeochem. Cycles 34. https://doi.org/10.1029/2020GB006649. . e2020GB006649.
Dahl, T.W., Boyle, R.A., Canfield, D.E., Connelly, J.N., Gill, B.C., Lenton, T.M., Bizzarro, M., 2014. Uranium isotopes distinguish two geochemically distinct stages during the later Cambrian SPICE event. Earth Planet. Sci. Lett. 401, 313–326. https://doi.org/10.1016/j.epsl.2014.05.043.
Dong, X., Zhang, H., 2017. Middle Cambrian through lowermost Ordovician conodonts from Hunan, South China. J. Paleontol. 91, 1–89. https://doi.org/10.1017/jpa.2015.43.
Dunk, R.M., Mills, R.A., Jenkins, W.J., 2002. A reevaluation of the oceanic uranium budget for the Holocene. Chem. Geol. 190, 45–67. https://doi.org/10.1016/S0009-2541(02)00110-9.
Egenhoff, S.O., Fishman, N.S., Ahlberg, P., Maletz, J., Jackson, A., Kolte, K., Lowers, H., Mackie, J., Newby, W., Petrowsky, M., 2015. Sedimentology of SPICE (Steptoean positive carbon isotope excursion): A high-resolution trace fossil and microfabric analysis of the middle to late Cambrian Alum Shale Formation, southern Sweden, in: Paying Attention to Mudrocks: Priceless!. Geological Society of America. https://doi.org/10.1130/2015.2515(05).
Farrell, Ú.C., Briggs, D.E.G., Gaines, R.R., 2011. Paleoecology of the olenid trilobite *triarthrus*: New evidence from beecher's trilobite bed and other sites of pyritization. Palaios 26, 730–742. https://doi.org/10.2110/palo.2011.p11-050r.
Fortey, R.A., 1989. There are extinctions and extinctions: examples from the Lower Palaeozoic. Philos. Trans. R. Soc. Lond. B 325, 327–355. https://doi.org/10.1098/rstb.1989.0092.
Frakes, L.A., Francis, J.E., Syktus, J.I., 1992. The Warm Mode: early Cambrian to late Ordovician. In: Climate Modes of the Phanerozoic. Cambridge University Press, pp. 7–14.
Freeman, R.L., Miller, J.F., Dattilo, B.F., 2018. Linguliform brachiopods across a Cambrian–Ordovician (Furongian, Early Ordovician) biomere boundary: the Sunwaptan–Skullrockian North American Stage boundary in the Wilberns and Tanyard formations of central Texas. J. Paleontol. 92, 751–767. https://doi.org/10.1017/jpa.2018.8.
Gill, B.C., Lyons, T.W., Young, S.A., Kump, L.R., Knoll, A.H., Saltzman, M.R., 2011. Geochemical evidence for widespread euxinia in the Later Cambrian ocean. Nature 469, 80–83. https://doi.org/10.1038/nature09700.
Goto, K.T., Anbar, A.D., Gordon, G.W., Romaniello, S.J., Shimoda, G., Takaya, Y., Tokumaru, A., Nozaki, T., Suzuki, K., Machida, S., Hanyu, T., Usui, A., 2014. Uranium isotope systematics of ferromanganese crusts in the Pacific Ocean: Implications for the marine ^{238}U/^{235}U isotope system. Geochim. Cosmochim. Acta 146, 43–58. https://doi.org/10.1016/j.gca.2014.10.003.
Guilbaud, R., Slater, B.J., Poulton, S.W., Harvey, T.H.P., Brocks, J.J., Nettersheim, B.J., Butterfield, N.J., 2018. Oxygen minimum zones in the early Cambrian ocean. Geochem. Perspect. Lett. 6, 33–38.
Hallam, A., Cohen, J.M., Chaloner, W.G., 1989. The case for sea-level change as a dominant causal factor in mass extinction of marine invertebrates. Philos. Trans. R. Soc. Lond. B 325, 437–455. https://doi.org/10.1098/rstb.1989.0098.
Harper, D.A.T., Topper, T.P., Cascales-Mi Nana, B., Servais, T., Zhang, Y.-D., Ahlberg, P., 2019. The Furongian (late Cambrian) Biodiversity Gap: Real or apparent? Palaeoworld 28, 4–12. https://doi.org/10.1016/j.palwor.2019.01.007.
He, Z., Clarkson, M.O., Andersen, M.B., Archer, C., Sweere, T.C., Kraal, P., Guthauser, A., Huang, F., Vance, D., 2021. Temporally and spatially dynamic redox conditions on an upwelling margin: the impact on coupled sedimentary Mo and U isotope systematics, and implications for the Mo-U paleoredox proxy. Geochim. Cosmochim. Acta 309, 251–271. https://doi.org/10.1016/j.gca.2021.06.024.
Herrmann, A.D., Gordon, G.W., Anbar, A.D., 2018. Uranium isotope variations in a dolomitized Jurassic carbonate platform (Tithonian; Franconian Alb, Southern Germany). Chem. Geol. 497, 41–53. https://doi.org/10.1016/j.chemgeo.2018.08.017.
Hinojosa, J.L., Stirling, C.H., Reid, M.R., Moy, C.M., Wilson, G.S., 2016. Trace metal cycling and ^{238}U/^{235}U in New Zealand's fjords: Implications for reconstructing global paleoredox conditions in organic-rich sediments. Geochim. Cosmochim. Acta 179, 89–109. https://doi.org/10.1016/j.gca.2016.02.006.
Holmden, C., Amini, M., Francois, R., 2015. Uranium isotope fractionation in Saanich Inlet: A modern analog study of a paleoredox tracer. Geochim. Cosmochim. Acta 153, 202–215. https://doi.org/10.1016/j.gca.2014.11.012.
Jaccard, S.L., Galbraith, E.D., 2012. Large climate-driven changes of oceanic oxygen concentrations during the last deglaciation. Nat. Geosci. 5, 151–156. https://doi.org/10.1038/ngeo1352.
Jost, A.B., Bachan, A., van de Schootbrugge, B., Lau, K.V., Weaver, K.L., Maher, K., Payne, J.L., 2017. Uranium isotope evidence for an expansion of marine anoxia during the end-Triassic extinction. Geochem. Geophys. Geosyst. 18, 3093–3108. https://doi.org/10.1002/2017GC006941.
Kaufman, A.J., Knoll, A.H., 1995. Neoproterozoic variations in the C-isotopic composition of seawater: Stratigraphic and biogeochemical implications. Precambrian Res. 73, 27–49. https://doi.org/10.1016/0301-9268(94)00070-8.
Krause, A.J., Mills, B.J.W., Zhang, S., Planavsky, N.J., Lenton, T.M., Poulton, S.W., 2018. Stepwise oxygenation of the Paleozoic atmosphere. Nat. Commun. 9, 4081. https://doi.org/10.1038/s41467-018-06383-y.
Landing, E., 2011. No Late Cambrian shoreline ice in Laurentia. GSA Today 21, e19. https://doi.org/10.1130/G113C.1.
Landing, E., 2012. Time-specific black mudstones and global hyperwarming on the Cambrian–Ordovician slope and shelf of the Laurentia palaeocontinent. Palaeogeogr. Palaeoclimatol. Palaeoecol. 367–368, 256–272. https://doi.org/10.1016/j.palaeo.2011.09.005.
Landing, E., Westrop, S.R., Adrain, J.M., 2011. The Lawsonian Stage - the *Eoconodontus notchpeakensis* FAD and HERB carbon isotope excursion define a globally correlatable terminal Cambrian stage. Bull. Geosci. 86, 621–640.
Landing, E., Ripperdan, R.L., Geyer, G., 2020. Uppermost Cambrian carbon chemostratigraphy: the HERB and undocumented TOCE events are not synonymous. Geol. Mag. 157, 1373–1377. https://doi.org/10.1017/S0016756820000382.
Lau, K.V., Maher, K., Altiner, D., Kelley, B.M., Kump, L.R., Lehrmann, D.J., Silva-Tamayo, J.C., Weaver, K.L., Yu, M., Payne, J.L., 2016. Marine anoxia and delayed Earth system recovery after the end-Permian extinction. Proc. Natl. Acad. Sci. U. S. A. 113, 2360–2365. https://doi.org/10.1073/pnas.1515080113.
Lau, K.V., Macdonald, F.A., Maher, K., Payne, J.L., 2017. Uranium isotope evidence for temporary ocean oxygenation in the aftermath of the Sturtian Snowball Earth. Earth Planet. Sci. Lett. 458, 282–292. https://doi.org/10.1016/j.epsl.2016.10.043.
Lau, K.V., Hancock, L.G., Severmann, S., Kuzminov, A., Cole, D.B., Behl, R.J., Planavsky, N.J., Lyons, T.W., 2022. Variable local basin hydrography and productivity control the uranium isotope paleoredox proxy in anoxic black shales. Geochim. Cosmochim. Acta 317, 433–456. https://doi.org/10.1016/j.gca.2021.10.011.
Lau, K.V., Lyons, T.W., Maher, K., 2020. Uranium reduction and isotopic fractionation in reducing sediments: Insights from reactive transport modeling. Geochim. Cosmochim. Acta 287, 65–92. https://doi.org/10.1016/j.gca.2020.01.021.
Li, D., Zhang, X., Chen, K., Zhang, G., Chen, X., Huang, W., Peng, S., Shen, Y., 2017. High-resolution C-isotope chemostratigraphy of the uppermost Cambrian stage (Stage 10) in South China: implications for defining the base of Stage 10 and palaeoenvironmental change. Geol. Mag. 154, 1232–1243. https://doi.org/10.1017/S0016756817000188.
Loch, J.D., Stitt, J.H., Derby, J.R., 1993. Cambrian–Ordovician boundary interval extinctions: implications of revised trilobite and brachiopod data from Mount Wilson, Alberta, Canada. J. Paleontol. 67, 497–517. https://doi.org/10.1017/S0022336000024859.
Matsumoto, K., 2007. Biology-mediated temperature control on atmospheric pCO_2 and ocean biogeochemistry. Geophys. Res. Lett. 34. https://doi.org/10.1029/2007GL031301.
McLennan, S.M., 2001. Relationships between the trace element composition of sedimentary rocks and upper continental crust. Geochem. Geophys. Geosyst. 2. https://doi.org/10.1029/2000GC000109.
Mei, M.-X., Wang, L., Li, Y.-Y., Peng, S.-C., Zhu, X.-J., Zuo, J.-X., 2019. Cyclostratigraphy within the framework of sequence stratigraphy for the Stage 10 of the Cambrian Furongian at the Wa'ergang section, Taoyuan County, Hunan Province (in Chinese with English abstract). J. Stratigr. 43, 115–132.
Miller, J.F., Ethington, R.L., Evans, K.R., Holmer, L.E., Loch, J.D., Popov, L.E., Repetski, J.E., Ripperdan, R.L., Taylor, J.F., 2006. Proposed stratotype for the base of the highest Cambrian stage at the first appearance datum of *Cordylodus andresi*, Lawson Cove section, Utah, USA. Palaeoworld 15, 384–405. https://doi.org/10.1016/j.palwor.2006.10.017.
Miller, J.F., Ripperdan, R.L., Loch, J.D., Freeman, R.L., Evans, K.R., Taylor, J.F., Tolbart, Z.C., 2015. Proposed GSSP for the base of Cambrian Stage 10 at the lowest occurrence of *Eoconodontus notchpeakensis* in the House Range, Utah, USA. Ann. Paléontol. 101, 199–211. https://doi.org/10.1016/j.annpal.2015.04.008.
Morford, J.L., Emerson, S.R., Breckel, E.J., Kim, S.H., 2005. Diagenesis of oxyanions (V, U, Re, and Mo) in pore waters and sediments from a continental margin. Geochim. Cosmochim. Acta 69, 5021–5032. https://doi.org/10.1016/j.gca.2005.05.015.
Palmer, A.R., 1965. Biomere: A new kind of biostratigraphic unit. J. Paleontol. 39, 149–153.
Palmer, A.R., 1984. The biomere problem: Evolution of an idea. J. Paleontol. 58, 599–611.
Peng, S., Babcock, L.E., Cooper, R.A., 2012. The Cambrian Period. In: Gradstein, F.M., Ogg, J.G., Schmitz, M.D., Ogg, G.M. (Eds.), The Geologic Time Scale 2012. Elsevier,

pp. 437–488.
Peng, S., Babcock, L.E., Zhu, X., Zuo, J., Dai, T., 2014. A potential GSSP for the base of the uppermost Cambrian stage, coinciding with the first appearance of *Lotagnostus americanus* at Wa'ergang, Hunan, China. GFF 136, 208–213. https://doi.org/10.1080/11035897.2013.865666.
Pohl, A., Lu, Z., Lu, W., Stockey, R.G., Elrick, M., Li, M., Desrochers, A., Shen, Y., He, R., Finnegan, S., Ridgwell, A., 2021. Vertical decoupling in Late Ordovician anoxia due to reorganization of ocean circulation. Nat. Geosci. 14, 868–873. https://doi.org/10.1038/s41561-021-00843-9.
Railsback, L.B., Ackerly, S.C., Anderson, T.F., Cisneti, J.L., 1990. Palaeontological and isotope evidence for warm saline deep waters in Ordovician oceans. Nature 343, 156. https://doi.org/10.1038/343156a0.
del Rey, Á., Havsteen, J.C., Bizzarro, M., Dahl, T.W., 2020. Untangling the diagenetic history of uranium isotopes in marine carbonates: A case study tracing the $\delta^{238}U$ composition of late Silurian oceans using calcitic brachiopod shells. Geochim. Cosmochim. Acta 287, 93–110. https://doi.org/10.1016/j.gca.2020.06.002.
Riedinger, N., Scholz, F., Abshire, M.L., Zabel, M., 2021. Persistent deep water anoxia in the eastern South Atlantic during the last ice age. Proc. Natl. Acad. Sci. U. S. A. 118. https://doi.org/10.1073/pnas.2107034118.
Ripperdan, R.L., 2002. The HERB event: End of Cambrian carbon cycle paradigm? Geol. Soc. Am. Programs Abstracts 413.
Ripperdan, R.L., Magaritz, M., Nicoll, R.S., Shergold, J.H., 1992. Simultaneous changes in carbon isotopes, sea level, and conodont biozones within the Cambrian-Ordovician boundary interval at Black Mountain, Australia. Geology 20, 1039–1042. https://doi.org/10.1130/0091-7613(1992)020<1039:SCICIS>2.3.CO;2.
Ripperdan, R.L., Magaritz, M., Kirschvink, J.L., 1993. Carbon isotope and magnetic polarity evidence for non-depositional events within the Cambrian–Ordovician boundary section near Dayangcha, Jilin Province, China. Geol. Mag. 130, 443–452. https://doi.org/10.1017/S0016756800020525.
Romaniello, S.J., Herrmann, A.D., Anbar, A.D., 2013. Uranium concentrations and $^{238}U/^{235}U$ isotope ratios in modern carbonates from the Bahamas: Assessing a novel paleoredox proxy. Chem. Geol. 362, 305–316. https://doi.org/10.1016/j.chemgeo.2013.10.002.
Runkel, A.C., Mackey, T.J., Cowan, C.A., Fox, D.L., 2010. Tropical shoreline ice in the late Cambrian: implications for Earth's climate between the Cambrian Explosion and the Great Ordovician Biodiversification Event. GSA Today 20, 4–10. https://doi.org/10.1130/GSATG84A.1.
Saltzman, M.R., Davidson, J.P., Holden, P., Runnegar, B., Lohmann, K.C., 1995. Sea-level-driven changes in ocean chemistry at an Upper Cambrian extinction horizon. Geology 23, 893–896. https://doi.org/10.1130/0091-7613(1995)023<0893:SLDCIO>2.3.CO;2.
Saltzman, M.R., Ripperdan, R.L., Brasier, M.D., Lohmann, K.C., Robison, R.A., Chang, W.T., Peng, S., Ergaliev, E.K., Runnegar, B., 2000. A global carbon isotope excursion (SPICE) during the Late Cambrian: relation to trilobite extinctions, organic-matter burial and sea level. Palaeogeogr. Palaeoclimatol. Palaeoecol. 162, 211–223. https://doi.org/10.1016/S0031-0182(00)00128-0.
Saltzman, M.R., Young, S.A., Kump, L.R., Gill, B.C., Lyons, T.W., Runnegar, B., 2011. Pulse of atmospheric oxygen during the late Cambrian. Proc. Natl. Acad. Sci. U. S. A. 108, 3876–3881. https://doi.org/10.1073/pnas.1011836108.
Saltzman, M.R., Edwards, C.T., Adrain, J.M., Westrop, S.R., 2015. Persistent oceanic anoxia and elevated extinction rates separate the Cambrian and Ordovician radiations. Geology 43, 807–810. https://doi.org/10.1130/G36814.1.
Schlesinger, W.H., Melack, J.M., 1981. Transport of organic carbon in the world's rivers. Tellus 33, 172–187. https://doi.org/10.3402/tellusa.v33i2.10706.
Scotese, C.R., 2021. An atlas of Phanerozoic paleogeographic maps: The seas come in and the seas go out. Annu. Rev. Earth Planet. Sci. 49, 679–728. https://doi.org/10.1146/annurev-earth-081320-064052.
Sheehan, P.M., 2001. History of marine biodiversity. Geol. J. 36, 231–249. https://doi.org/10.1002/gj.890.
Sial, A.N., Peralta, S., Gaucher, C., Toselli, A.J., Ferreira, V.P., Frei, R., Parada, M.A., Pimentel, M.M., Pereira, N.S., 2013. High-resolution stable isotope stratigraphy of the upper Cambrian and Ordovician in the Argentine Precordillera: carbon isotope excursions and correlations. Gondwana Res. 24, 330–348. https://doi.org/10.1016/j.gr.2012.10.014.
Sigman, D.M., Hain, M.P., Haug, G.H., 2010. The polar ocean and glacial cycles in atmospheric CO_2 concentration. Nature 466, 47. https://doi.org/10.1038/nature09149.
Stirling, C.H., Andersen, M.B., Potter, E.-K., Halliday, A.N., 2007. Low-temperature isotopic fractionation of uranium. Earth Planet. Sci. Lett. 264, 208–225. https://doi.org/10.1016/j.epsl.2007.09.019.
Stitt, J.H., 1971. Repeating evolutionary pattern in late Cambrian trilobite biomeres. J. Paleontol. 45, 178–181.
Stitt, J.H., 1975. Adaptive radiation, trilobite paleoecology, and extinction, Ptychaspidid Biomere, Late Cambrian of Oklahoma. Fossils Strata 4, 381–390.
Taylor, J.F., 2006. History and status of the biomere concept. Mem. Assoc. Australas. Palaeontol. 247–265.
Tissot, F.L.H., Chen, C., Go, B.M., Naziemiec, M., Healy, G., Bekker, A., Swart, P.K., Dauphas, N., 2018. Controls of eustasy and diagenesis on the $^{238}U/^{235}U$ of carbonates and evolution of the seawater ($^{234}U/^{238}U$) during the last 1.4 Myr. Geochim. Cosmochim. Acta 242, 233–265. https://doi.org/10.1016/j.gca.2018.08.022.
Tostevin, R., Clarkson, M.O., Gangl, S., Shields, G.A., Wood, R.A., Bowyer, F., Penny, A.M., Stirling, C.H., 2019. Uranium isotope evidence for an expansion of anoxia in terminal Ediacaran oceans. Earth Planet. Sci. Lett. 506, 104–112. https://doi.org/10.1016/j.epsl.2018.10.045.
Trotter, J.A., Williams, I.S., Barnes, C.R., Lécuyer, C., Nicoll, R.S., 2008. Did cooling oceans trigger Ordovician biodiversification? Evidence from conodont thermometry. Science 321, 550–554. https://doi.org/10.1126/science.1155814.
Tyson, R.V., Pearson, T.H., 1991. Modern and ancient continental shelf anoxia: an overview. Geol. Soc. London Spec. Publ. 58, 1–24. https://doi.org/10.1144/GSL.SP.1991.058.01.01.
Westrop, S.R., Ludvigsen, R., 1987. Biogeographic control of trilobite mass extinction at an upper Cambrian "biomere" boundary. Paleobiology 13, 84–99.
Weyer, S., Anbar, A.D., Gerdes, A., Gordon, G.W., Algeo, T.J., Boyle, E.A., 2008. Natural fractionation of $^{238}U/^{235}U$. Geochim. Cosmochim. Acta 72, 345–359. https://doi.org/10.1016/j.gca.2007.11.012.
White, D.A., Elrick, M., Romaniello, S., Zhang, F., 2018. Global seawater redox trends during the Late Devonian mass extinction detected using U isotopes of marine limestones. Earth Planet. Sci. Lett. 503, 68–77. https://doi.org/10.1016/j.epsl.2018.09.020.
Wood, R., Erwin, D.H., 2018. Innovation not recovery: dynamic redox promotes metazoan radiations. Biol. Rev. 93, 863–873. https://doi.org/10.1111/brv.12375.
Wotte, T., Strauss, H., 2015. Questioning a widespread euxinia for the Furongian (Late Cambrian) SPICE event: indications from $\delta^{13}C$, $\delta^{18}O$, $\delta^{34}S$ and biostratigraphic constraints. Geol. Mag. 152, 1085–1103. https://doi.org/10.1017/S0016756815000187.
Zhang, F., Algeo, T.J., Romaniello, S.J., Cui, Y., Zhao, L., Chen, Z.-Q., Anbar, A.D., 2018. Congruent Permian-Triassic $\delta^{238}U$ records at Panthalassic and Tethyan sites: Confirmation of global-oceanic anoxia and validation of the U-isotope paleoredox proxy. Geology 46, 327. https://doi.org/10.1130/G39695.1.
Zhang, F., Algeo, T.J., Cui, Y., Shen, J., Song, H., Sano, H., Rowe, H.D., Anbar, A.D., 2019. Global-ocean redox variations across the Smithian-Spathian boundary linked to concurrent climatic and biotic changes. Earth-Sci. Rev. 195, 147–168. https://doi.org/10.1016/j.earscirev.2018.10.012.
Zhang, F., Shen, S., Cui, Y., Lenton, T.M., Dahl, T.W., Zhang, H., Zheng, Q., Wang, W., Krainer, K., Anbar, A.D., 2020. Two distinct episodes of marine anoxia during the Permian-Triassic crisis evidenced by uranium isotopes in marine dolostones. Geochim. Cosmochim. Acta 287, 165–179. https://doi.org/10.1016/j.gca.2020.01.032.
Zheng, Y., Anderson, R.F., van Geen, A., Fleisher, M.Q., 2002. Preservation of particulate non-lithogenic uranium in marine sediments. Geochim. Cosmochim. Acta 66, 3085–3092. https://doi.org/10.1016/S0016-7037(01)00632-9.
Zhu, M., Babcock, L.E., Peng, S., Ahlberg, P., 2021. Reply to 'Uppermost Cambrian carbon chemostratigraphy: the HERB and undocumented TOCE events are not synonymous'. Geol. Mag. 158, 1323–1326. https://doi.org/10.1017/S0016756820001120.
Zhu, M.-Y., Babcock, L.E., Peng, S.-C., 2006. Advances in Cambrian stratigraphy and paleontology: Integrating correlation techniques, paleobiology, taphonomy and paleoenvironmental reconstruction. Palaeoworld 15, 217–222. https://doi.org/10.1016/j.palwor.2006.10.016.
Zhuravlev, A.Yu., 2001. Biotic diversity and structure during the Neoproterozoic–Ordovician transition. In: Zhuravlev, A., Riding, R. (Eds.), The Ecology of the Cambrian Radiation. Columbia University Press.